Relation between stability and resilience determines the performance of early warning signals under different environmental drivers

Lei Dai[a,1,2], Kirill S. Korolev[b], and Jeff Gore[a]

[a]Department of Physics, Physics of Living Systems Group, Massachusetts Institute of Technology, Cambridge, MA 02139; and [b]Department of Physics and Program in Bioinformatics, Boston University, Boston, MA 02215

Edited by Stephen R. Carpenter, University of Wisconsin, Madison, WI, and approved June 19, 2015 (received for review September 23, 2014)

Shifting patterns of temporal fluctuations have been found to signal critical transitions in a variety of systems, from ecological communities to human physiology. However, failure of these early warning signals in some systems calls for a better understanding of their limitations. In particular, little is known about the generality of early warning signals in different deteriorating environments. In this study, we characterized how multiple environmental drivers influence the dynamics of laboratory yeast populations, which was previously shown to display alternative stable states [Dai et al., *Science*, 2012]. We observed that both the coefficient of variation and autocorrelation increased before population collapse in two slowly deteriorating environments, one with a rising death rate and the other one with decreasing nutrient availability. We compared the performance of early warning signals across multiple environments as "indicators for loss of resilience." We find that the varying performance is determined by how a system responds to changes in a specific driver, which can be captured by a relation between stability (recovery rate) and resilience (size of the basin of attraction). Furthermore, we demonstrate that the positive correlation between stability and resilience, as the essential assumption of indicators based on critical slowing down, can break down in this system when multiple environmental drivers are changed simultaneously. Our results suggest that the stability–resilience relation needs to be better understood for the application of early warning signals in different scenarios.

early warning signals | population collapse | environmental drivers | stability–resilience relation

Complex systems are often subject to multiple environmental drivers. Microenvironmental cues such as growth factors and drug concentrations control the progression of cancer cells (1). Parasites, insecticides, and habitat destruction have all been blamed for the rapid decline of honey bee colonies in the North America (2). The global biodiversity is influenced by factors including habitat fragmentation, climate change, etc. For a system with alternative stable states (3, 4), pressure on an environmental driver pushes the system closer to a tipping point (5, 6). Once the driver crosses a certain threshold, the system goes through a critical transition and shifts to a different state [e.g., the malignant behavior of cancer (1), the collapse of pollinator populations (7), or a large-scale mass extinction (8, 9)].

There has been a growing interest in developing a toolbox of early warning signals to avoid such undesirable transitions (10–17). Theoretical and empirical studies have found that signatures of "critical slowing down" in the spatiotemporal dynamics may be used to indicate impending tipping points (18–29). These indicators are based on the fact that the dynamics around the equilibrium of a system slows down near a tipping point (19, 30, 31). This would lead to an increase in recovery time from perturbations or changes in the pattern of fluctuations (e.g., increases in variation and autocorrelation) (20, 32). The appeal of these generic indicators is that they do not rely on detailed knowledge of a complex system, thus complementing the use of system-specific modeling to determine when critical transitions may occur. However, the failure of early warning signals before certain transitions has raised concerns on their generality (33, 34). In some cases, the failure of detection is merely a statistical problem, e.g., insufficient quality or quantity of data. The real concern, however, is that critical slowing down does not precede all types of transitions. In two recent reviews (35, 36), the authors summarize the potential of observing critical slowing down before regime shifts caused by different mechanisms. They also highlighted the need for a better understanding of the limitation of our current toolbox, which would aid the application to real-world scenarios.

One gap in our understanding is the generality of early warning signals in a system subject to multiple environmental drivers. Previous experimental studies have focused solely on transitions induced by a single, specific driver. In this study, we tune multiple environmental drivers in laboratory yeast populations, which have been shown to display cooperative growth and alternative stable states under daily dilution (22, 37). To overcome the difficulty in comparing early warning signals between different deteriorating environments, we propose to evaluate them as "indicators for loss of resilience." Finally, we find that the relation between stability and resilience determines the performance of statistical indicators and provides further insight to their limitation.

Results

We pushed yeast populations to collapse by slowly tuning two different environmental drivers (Fig. 1). We grew yeast cells in

Significance

Alternative stable states and critical transitions are widespread in nature and can have profound consequences for conservation, climate changes, and human health. Our current toolbox of early warning signals before critical transitions has seen both successes and failures. Understanding the limitations of these indicators is crucial for application in real-world scenarios. In this study, we explored the population dynamics of laboratory yeast under different forms of environmental deterioration. We found that the performance of early warning signals under different environmental drivers is determined by the underlying relation between stability and resilience. This work presents a framework to evaluate the utility of early warning signals, and it sets a foundation for further studies on how dynamical systems respond to environmental changes.

Author contributions: L.D., K.S.K., and J.G. designed research; L.D. performed research; L.D. analyzed data; and L.D., K.S.K., and J.G. wrote the paper.

The authors declare no conflict of interest.

This article is a PNAS Direct Submission.

Data deposition: The data reported in this paper have been deposited in the Dryad database, datadryad.org (10.5061/dryad.k30v3).

[1]To whom correspondence should be addressed. Email: leidai@ucla.edu.

[2]Present address: Department of Ecology and Evolutionary Biology, University of California, Los Angeles, CA 90095.

This article contains supporting information online at www.pnas.org/lookup/suppl/doi:10.1073/pnas.1418415112/-/DCSupplemental.

batch culture using synthetic media supplemented with sugar sucrose; on each day the cells were diluted and transferred into fresh media. As demonstrated previously (22, 23), yeast populations experience a tipping point (fold bifurcation) leading to sudden collapse as a result of the cooperative breakdown of sucrose outside of the cell. The first driver is the dilution factor used for daily transfer into fresh media (Fig. 1*A*). After an initial period of 4 days to stabilize the yeast populations at a dilution factor of 500, we increased the dilution factor by 10% per day and pushed populations to collapse in a few weeks (Fig. 1*B*). The steady increase in dilution factor mimics a rising death rate. Consistent with previous experimental measurements probing this environmental driver (22), we found that both the coefficient of variation (CV) and autocorrelation time of the deteriorating-environment group increased substantially before the estimated tipping point (*SI Appendix*, Fig. S1), whereas no increase in these indicators was observed in the constant-environment group with a fixed dilution factor of 500 (Fig. 1 *C* and *D*). In the second deteriorating environment, we imposed increasingly severe nutrient limitation by reducing the sucrose concentration by 20% per day (Fig. 1*E*). The yeast populations collapsed in a similar fashion over the course of 3 wk (Fig. 1*F*). In this case, we also observed increases in CV and autocorrelation time before population collapse (Fig. 1 *G* and *H*), although the warning signals were not as pronounced as those seen with an increasing dilution factor. Consistent with visual inspection (Fig. 1 *C*, *D*, *G*, and *H*), for both statistical indicators the Kendall's τ coefficient under increasing dilution factor (CV: $\tau = 0.71$, $P = 6.7 \times 10^{-5}$; autocorrelation time: $\tau = 0.27$, nonsignificant) is larger than those under decreasing sucrose availability (CV: $\tau = 0.59$, $P = 2.2 \times 10^{-4}$; autocorrelation time: $\tau = 0.09$, nonsignificant).

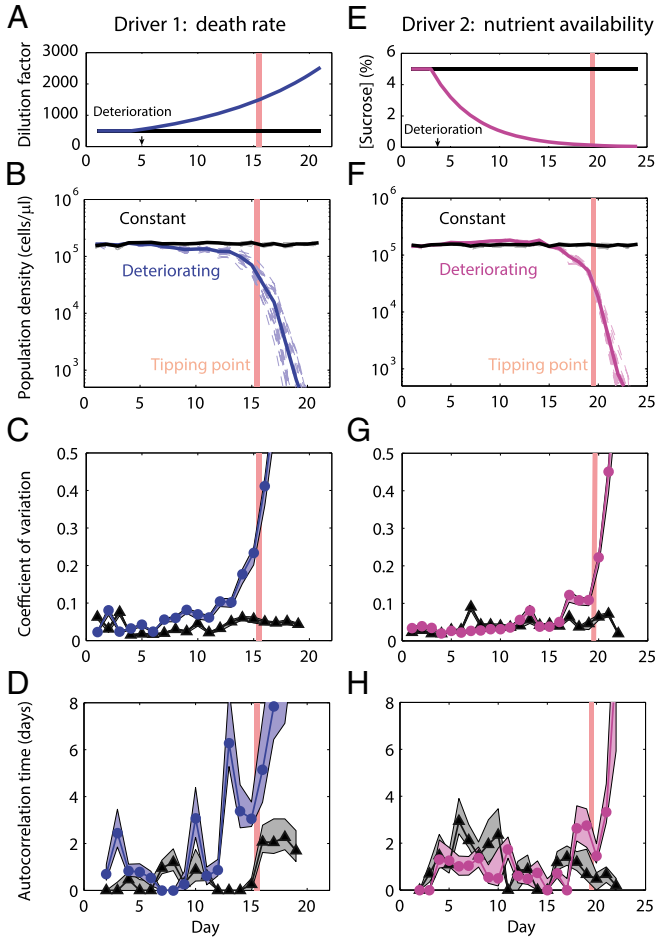

Fig. 1. Increased variation and autocorrelation time in population density were observed before population collapse in two different deteriorating environments. (*A*) A slowly deteriorating environment with a rising death rate. Dilution factor of the constant-environment group (black) was fixed at 500. After an initial phase of 4 d to stabilize the populations, the dilution factor of the deteriorating-environment group (blue) was increased from 500 to over 2,500 (*SI Appendix*, Table S1). The red line marks the estimated day when the populations crossed a tipping point (*SI Appendix*, Fig. S1). (*B*) Population density of individual replicates (dashed lines) and the mean population density among replicates (solid line) over time. Coefficient of variation (*C*) and autocorrelation time (*D*) of the deteriorating-environment group (circle) increased substantially at least 3 d in advance. The indicators for the constant-environment group (triangle) did not show any trend. The shaded regions for the indicators correspond to the 25–75% confidence interval given by bootstrap. (*E–H*) A slowly deteriorating environment with decreasing nutrient availability. Conventions for symbols are the same as in *A–D*.

Our empirical observation of early warning signals before population collapse under two drivers is encouraging for the use of these indicators in a system subject to different forms of stress. Nevertheless, the clear difference in the performance of the indicators across the two deteriorating environments is not well understood. In real-time deteriorating environments, the performance of early warning signals can be complicated by the rate of environmental changes. For example, an abruptly large shift in the environment can clearly push the system to an alternative state before it is possible to observe any warning signal. To exclude any effect caused by the rate of environmental changes, we characterized the dynamics of yeast populations over a range of fixed environmental conditions. Such an experiment can be considered as an infinitely slowly deteriorating environment, thus allowing us to compare the strength of the early warning indicators without the complexity introduced by potentially different rates of environmental deterioration. We experimentally mapped out the bifurcation diagram for sucrose availability and observed a fold bifurcation at low concentration of sucrose (Fig. 2*B*). A similar bifurcation diagram for dilution factor was mapped in our previous study (Fig. 2*A*) (22). We then tracked the fluctuations around the equilibrium and measured statistical indicators over an ensemble of replicate populations. Under both environmental drivers, CV (Fig. 2 *C* and *D*) and autocorrelation time (*SI Appendix*, Fig. S2 *A* and *B*) of yeast population increased before the fold bifurcation.

Because the proximity to a fold bifurcation is measured by the unit of a specific driver (dilution factor or sucrose concentration), we cannot directly compare the performance of statistical indicators across multiple environments as a function of the underlying driver. In fact, we cannot necessarily say that the early warning indicators perform better under increasing dilution than under decreasing sucrose concentrations, because the indicators would presumably get stronger if the sucrose concentration was closer to the threshold at the critical transition.

Here we propose to evaluate the early warning signals before a fold bifurcation with respect to the underlying loss of resilience. For the yeast populations, we define resilience as the distance between the stable and unstable fixed points (Fig. 2 *A* and *B*), which measures the maximal pulse perturbation (i.e., the number of individuals lost) a population can tolerate without going extinct. This definition of resilience therefore has a natural interpretation relative to environmental perturbations and also corresponds to the (one-sided) size of the basin of attraction of the stable state. In our system, we have experimentally mapped out the bifurcation diagrams with two different environmental drivers, thus allowing for a direct measure of resilience. As the pressure on a driver increases, a population loses resilience approaching the fold bifurcation. Right at the fold bifurcation, resilience is reduced to zero as the stable and unstable fixed points meet and "collide."

With the experimental bifurcation diagrams mapped out, we can quantify the performance of early warning signals as a function

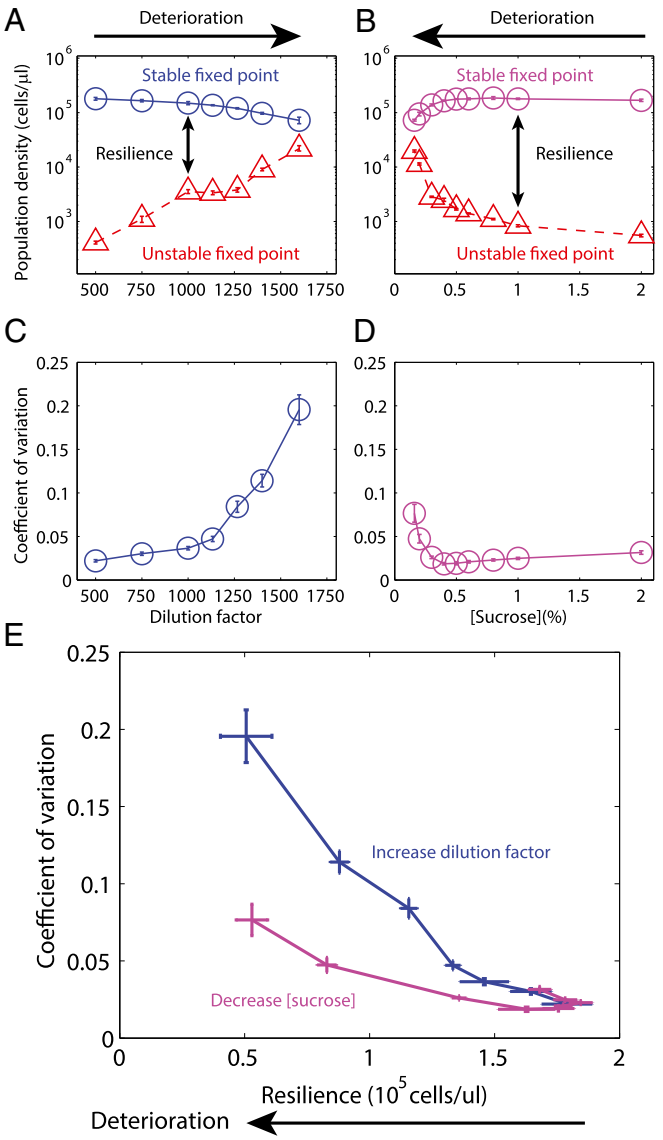

Fig. 2. Early warning signals can be viewed as resilience indicators. (*A* and *B*) Bifurcation diagrams were mapped under two different environmental drivers: dilution factor (*A*) and sucrose (*B*). (*C* and *D*) Coefficient of variation (CV) increased as environment deteriorated with increasing dilution factor (*C*) or decreasing sucrose concentration (*D*). *A* and *C* are reprinted with permission from ref. 22. (*E*) To compare the performance of warning signals under different environmental drivers, we evaluated CV as a function of resilience. Given that the same amount of resilience is lost, the increase in CV was indeed more substantial with increasing dilution factor than with decreasing sucrose concentration. Error bars are SEs given by bootstrap.

of resilience and compare them across environments (Fig. 2*E*). Given the same loss of population resilience, we found that the CV increased more under dilution stress compared with sucrose stress. The comparison for autocorrelation time across the two environments yielded similar results (*SI Appendix*, Fig. S2*C*). This analysis of early warning signals as indicators for loss of resilience suggested that the previously observed difference in their performance across multiple deteriorating environments could not be necessarily explained by how fast we tuned the drivers (Fig. 1) nor how close we were to the bifurcation (Fig. 2 *C* and *D*). Instead, the varying performance of the early warning indicators reflected an intrinsic difference in the response of yeast populations to different environmental drivers (*SI Appendix*, Fig. S10).

To understand how a dynamical system can respond to drivers differently and the implications for early warning signals, we need to examine resilience and stability (38–40), the two fundamental properties underlying the dynamics of a system (Fig. 3). Mathematical definitions of these two properties and alternative terminology in the literature are summarized in *SI Appendix*, Table S2. Resilience, as determined by the basin of attraction, is a measure of a system's tolerance to large perturbations (38, 41–43) (Fig. 3 *A* and *B*). As can be seen in the experimental bifurcation diagrams (Fig. 2 *A* and *B*), resilience is reduced to zero at a tipping point (fold bifurcation). Stability, or recovery rate, on the other hand, measures how fast a system recovers to its stable fixed point after small perturbations (Fig. 3 *A* and *B*). As a result of critical slowing down, stability decreases to zero approaching a fold bifurcation. The time needed to recover from perturbations becomes longer (19, 31), hence the system becomes more correlated with its past (32); moreover, the perturbations accumulate and lead to an increase in the size of the fluctuations (20). Statistical indicators such as CV and autocorrelation time, which characterize the pattern of fluctuations, are manifestations of stability (*SI Appendix*, *Text S1*). Thus, using increases in CV and autocorrelation time to indicate loss of resilience is based on the assumption that changes in stability are positively correlated with changes in resilience as the environment deteriorates (*SI Appendix*, *Text S2*).

We speculate that the relation between stability and resilience determines the performance of early warning signals under different environmental drivers (Fig. 4*A*). Starting from a good initial condition with high resilience and high stability (i.e., a wide and steep potential well), changes in a driver can push the system to a fold bifurcation. At the bifurcation, both resilience and stability are reduced to zero. On a stability–resilience diagram, the approach of a fold bifurcation through increasing pressure on a driver can be visualized as a path connecting the initial condition and the origin

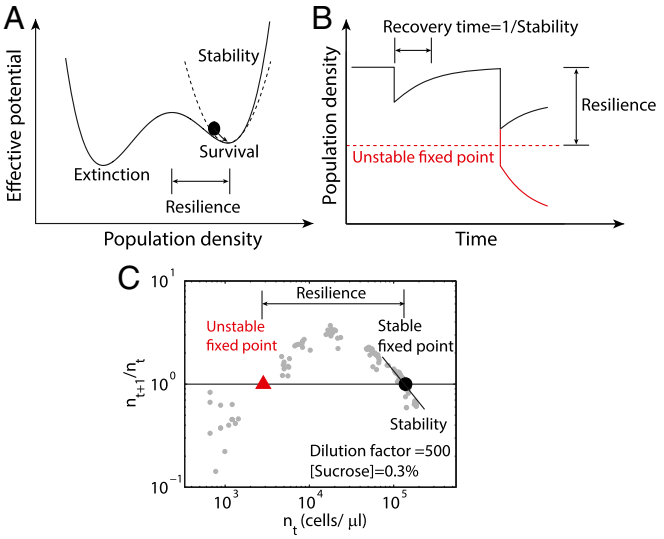

Fig. 3. Stability and resilience are two fundamental properties of dynamical systems. (*A*) A one-dimensional dynamical system can be represented by an effective potential. The state variable is population density in our system. Here we illustrate a bistable system (population survival and extinction). The bottom and the top of the potential represent stable and unstable fixed points, respectively. Resilience is determined by the (one-sided) size of basin of attraction. Stability is determined by the curvature at the stable fixed point. (*B*) In our system, we define resilience as the maximal perturbation (i.e., number of individuals lost) a population can withstand without going extinct. Stability is defined as the return rate to the stable fixed point after small perturbations. (*C*) We extracted stability and resilience from the daily growth profile of yeast populations (*SI Appendix*, *Supplementary Methods*).

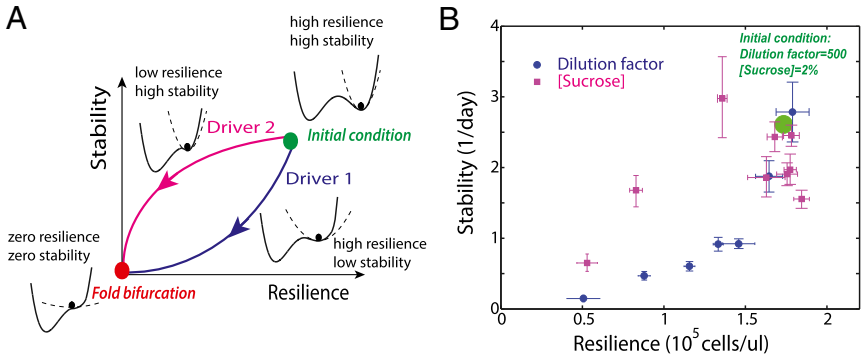

Fig. 4. Stability–resilience relation under different environmental drivers. (*A*) Starting from an initial condition with high resilience and high stability (green dot), pressure on an environmental driver pushes the system toward a fold bifurcation (red dot) where both resilience and stability are reduced to zero. Along such a path, changes in the dynamics can be visualized by a changing potential landscape. Loss of resilience corresponds to shrinkage in the basin of attraction, whereas loss of stability leads to a flattened curvature around the bottom of the potential. The exact path taken can vary between drivers. (*B*) Stability–resilience relation under the two experimental drivers in yeast populations. Starting from the same initial condition (green dot), the loss of stability under increasing dilution factor is greater than that under decreasing sucrose, given the same loss of resilience. This explains the observed difference in the performance of CV and autocorrelation time under the two drivers. Error bars are SEs given by bootstrap.

(resilience = 0, stability = 0). For different drivers leading to a fold bifurcation, the system will always end at the origin with zero resilience and zero stability. Nevertheless, it is plausible that the precise path taken (i.e., the exact relation between stability and resilience) can vary between drivers. For example, under one environmental deterioration ("driver 1"), the system may lose much stability while maintaining a high resilience (a wide but flattened potential well). On the other hand, a different form of environmental deterioration ("driver 2") may result in a significant loss of resilience with little reduction in stability (a narrow but steep potential well). Therefore, given the same loss of resilience, the loss of stability under driver 1 is always greater than that under driver 2 (Fig. 4*A*). Environmental perturbations such as severe weather will often cause a complex system to transition before the deterministic bifurcation point (10, 17, 44), meaning that it is important for early warning signals to precede a severe loss of resilience. As resilience is reduced, a large external perturbation is more likely to push a population below its extinction threshold (i.e., the unstable fixed point). Given this need to maintain a minimal resilience, the early warning indicators based on loss of stability will be more effective for driver 1 compared with driver 2 as a result of their different paths on the stability–resilience diagram.

To confirm our hypothesis, we measured the relation between stability and resilience for yeast populations under two drivers: dilution factor and sucrose concentration. For a given environmental condition, we determined resilience and stability from the deterministic growth profile (Fig. 3*C*). Indeed, we found that the stability–resilience relation was dependent on the driver (Fig. 4*B*). Yeast populations lost resilience and approached a fold bifurcation with either an increase in dilution factor or a decrease in sucrose concentration. However, with an increasing dilution factor, populations lost stability more rapidly, which explained why the early warning signals based on loss of stability had a better performance under environmental deterioration induced by this driver.

In addition, we measured the dynamics of yeast populations under a third environmental driver, osmotic stress caused by salt (NaCl). Our yeast populations again lost both stability and resilience at higher concentration of salt, before eventually reaching a fold bifurcation (*SI Appendix*, Fig. S3). The exact path of this driver on the stability–resilience diagram was observed to be between the paths of dilution factor and sucrose. As the environment deteriorates with an increasing concentration of salt, we found that changes in statistical indicators as a function of resilience were also intermediate among the three drivers. Thus, our data supported the hypothesis that the performance of early warning signals under different environmental drivers was governed by the relation between stability and resilience.

The stability–resilience relation also informs us of possible scenarios under which early warning signals will fail (Fig. 5). On a stability–resilience diagram, we can find environmental conditions that display a tradeoff between resilience and stability (Fig. 4*B* and *SI Appendix*, Fig. S4*A*). This tradeoff demonstrates that the positive correlation between stability and resilience breaks down in this system when multiple drivers are changed simultaneously. We simulated a simple phenomenological model of yeast populations, which had been shown to capture the cooperative growth dynamics and bistability in our system (*SI Appendix*, *Supplementary Methods*) (22). We tuned two parameters as environmental drivers, dilution factor and the carrying capacity. As expected, changing an individual parameter of the model corresponds to a path on the stability–resilience diagram (Fig. 5*A*). We also simulated another scenario in which the growth rate during slow growth phase was decreased (*SI Appendix*, Fig. S5). In our experiment, lowering the sucrose concentration would limit the carrying capacity as well as how fast yeast cells grow at low cell densities. So the outputs of our model were consistent with the experimental observation that tuning sucrose concentration led to a less convex path than tuning dilution factor. Surprisingly, when we tuned two parameters simultaneously in opposite directions (i.e., the pressure on one driver increased while it decreased on the other), we found that under certain conditions, a population can lose resilience while gaining stability (Fig. 5*A*). In this case, as the population becomes less resilient (i.e., approaching a fold bifurcation), the warning signals would actually fade away because of the increase in stability. To illustrate how anticorrelation between stability and resilience may occur, we used our model to plot contours of stability and resilience in the parameter space of the two drivers (Fig. 5*B* and *SI Appendix*, Fig. S4*B*). If the two contours intersect, it is possible to alter the environmental drivers together along certain directions such that changes in stability and resilience are inversely correlated (*SI Appendix*, Fig. S4*C* and *Text S3*). Thus, this phenomenon is not specific to our system; rather it is likely a general scenario for systems under the influence of multiple environmental drivers.

Discussion

We have proposed to evaluate critical slowing down indictors before a fold bifurcation with respect to the underlying loss of resilience, and we have shown that the stability–resilience relation can vary between different environmental drivers. Resilience, which is defined on state space instead of parameter space, provides a metric

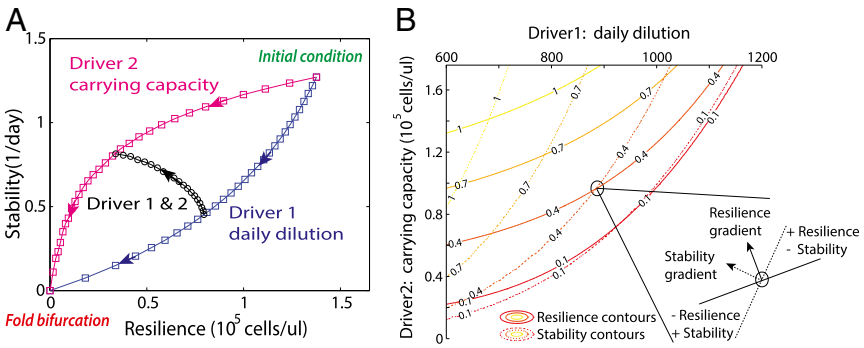

Fig. 5. Anticorrelation between stability and resilience is possible when multiple drivers are changed simultaneously in a phenomenological model of yeast populations. (*A*) Three scenarios were simulated: (*i*) a gradual increase in dilution factor (blue sqaures), (*ii*) a gradual decrease in carrying capacity (magenta squares), and (*iii*) a decrease in carrying capacity together with a decrease in dilution factor (black circles). With simultaneous changes of two drivers in opposite directions (*SI Appendix*, Table S3), we observed that stability and resilience can be anticorrelated. (*B*) Simulated resilience contours (solid lines) and stability contours (dashed lines) in the parameter space of two drivers. If the two contours intersect (black circle), the system can lose resilience while gaining stability (or vice versa) with simultaneous changes of two drivers (*Inset*). The units of stability and resilience are the same as labeled in *A*.

for the distance to a fold bifurcation when multiple drivers are involved. More than being a convenient metric, resilience is an important property of the population, which together with stability determines the likelihood of extinction due to demographic or environmental noise. The utility of early warning indicators is therefore at least partially related to their ability to predict both changes in stability and resilience, assuming a positive correlation between these two metrics (19, 36).

In practice, we need to observe changes in indicators before resilience and stability become so small that stochastic transitions occur (44, 45). Moreover, to take actions to reverse the environmental deterioration requires a sufficiently early detection of warning signals. The successful detection of warning signals is determined by many factors, such as the magnitude of external perturbations, the sampling frequency, etc. In our study, we find that the utility of warning signals also depends on a system's response to specific environmental drivers. Although different drivers are known to differ in their threat to populations or ecological systems, previous work has attributed that largely to the distance to bifurcation or the degree of deterioration, whereas we show that the intrinsic difference between environmental drivers is at least equally important. We expect more loss of stability and a larger increase in statistical indicators along a more convex path on the stability–resilience diagram (driver 1, Fig. 4*A*) than a concave path (drive 2). This observation does not depend on the location of the starting condition, i.e., distance from the bifurcation (*SI Appendix*, Fig. S9*A*). In addition, the shape of the stability–resilience relation determines how rapidly the critical slowing down indicators would increase as a function of loss of resilience under a specific driver. Along a concave curve, the slope becomes steeper near the bifurcation, so one might be tempted to think that the increase in indicators would become more visible immediately before the transition. However, we should be aware that warning indicators need to be observed before the deterministic bifurcation (*SI Appendix*, Fig. S9*B*), i.e., before a complete loss of resilience. Indeed, large environmental perturbations (e.g., external forcing events) can push populations below the critical level if the resilience is too small. Alternatively, extinctions can be triggered by repeated small perturbations due to environmental or demographic noise, and in this case, both stability and resilience need to be large to avoid stochastic extinction (*SI Appendix*, Fig. S9*C*). In both scenarios, however, changes in driver 1 lead to the greater loss of stability (i.e., stronger warning signals), given the same increase in the risk of extinction.

In addition to the difficulty of detecting warning signs in time, we should be aware of possible scenarios of false negatives. Failures of indicators based on critical slowing down have been discussed in a few contexts (33–35, 46). To use changes in the pattern of fluctuations (or a decrease in recovery rate) to indicate loss of resilience is based on the assumption that there is a positive correlation between changes in stability and resilience. Our finding of anticorrelation under multiple drivers may seem nonintuitive, as we are accustomed to extrapolate the positive correlation near a bifurcation (as a result of critical slowing down) to conditions further away from the bifurcation. Such extrapolations have been supported by theoretical (19) and empirical (22, 24) work in various systems; however, previous studies largely ignored the possibility that more than one driver can be involved in environmental changes. Our analysis suggests that early warning signals may fail more frequently when two drivers are changed in opposite directions (for example, a wildlife population subject to continued habitat fragmentation but less killing by humans). In principle, even a single driver may cause loss of resilience with no decrease in stability (*SI Appendix*, *Text S3*), although we did not observe this in our system. We believe that understanding the limitation of our current toolbox of warning indicators will help us make better decisions on when and how to apply them.

One interesting question that begs future studies is how to use the stability–resilience analysis to inform the performance of indicators in other systems, where we usually cannot measure the stability–resilience relation directly or no parameterized model is available. It is worth noting that to map and compare stability–resilience curves does not require perfect knowledge of the system. For example, we simulated the stability–resilience relation under sucrose reduction by decreasing carrying capacity or decreasing the growth rate at low cell density, which is a crude approximation of how sucrose reduction affects growth of yeast cells. Nevertheless the model outputs were able to reproduce the qualitative pattern in experimental data. This suggests that perhaps one way to apply our analysis to other systems is through a model-based approach. Even for systems with relatively little information, models that only capture the structure of a system (47) may be sufficient to infer the stability–resilience relation. Moreover, studying a range of ecological models may inform us whether there is any general pattern between the type of environmental driver and the shape of stability–resilience relation, such as which drivers tend to allow strong warning signals.

To use the stability–resilience framework to study the dynamical behavior of complex systems, one important consideration is how to choose appropriate metrics. Defining resilience for systems with higher dimensions is not always straightforward, especially when the basin of attraction has a complex geometry (34). In our one-dimensional system (single species), we quantified resilience as the

distance between stable and unstable fixed points, which is the number of individuals a population with a strong Allee effect (48) can lose without going extinct deterministically. However, if perturbations are proportional to the total abundance, then the ratio between stable and unstable fixed points may be a more appropriate metric, which is essentially the distance between stable and unstable fixed points for log transformed abundance. The proper metric for resilience therefore depends on both the intrinsic properties of a system and also the nature of the environmental perturbations.

In our study, we find that the exact relation between recovery rate and the size of the basin of attraction is dependent on the environmental driver. This improves our understanding of when we may rely on knowledge about the local properties around equilibrium to infer changes in the global properties of a dynamical system. If we have some prior knowledge about a specific system, one strategy to look for warning indicators is to identify properties that change monotonically under environmental deterioration. For example, equilibrium population size will decline before a transcritical bifurcation, so a small population can be considered as a warning signal. The motivation for ongoing studies on critical slowing down indicators, among many other warning signals, is to identify their potential as well as their limitations (26) and develop a toolbox of indicators. Investigations into other properties [e.g., resistance (49), reactivity (50, 51), invasiveness, etc.] and their relations will help us address a fundamental question: how to measure the "stability" of a system (52, 53). A better assessment of complex ecosystems may guide our efforts to avoid systemic risks of financial networks (54), engineer a healthy gut microbiota (55), and cope with regime shifts in the environment (9).

Materials and Methods

We grew the budding yeast *Saccharomyces cerevisiae* in 200 μL batch culture at 30 °C using synthetic media supplemented with variable concentrations of sucrose (22). Serial dilutions were performed daily with variable dilution factors. Population densities were recorded each day by measuring optical density.

Statistical indicators were calculated at each observation time over an ensemble of replicate populations. We extracted stability and resilience from the daily growth profile of yeast populations. Simulations were based on a phenomenological model of yeast populations with two phases of daily growth: a slow exponential growth phase at low cell densities, followed by a logistic growth phase with a higher per capita growth rate at intermediate cell densities. Full details are available in *SI Appendix, Supplementary Methods*.

ACKNOWLEDGMENTS. The authors thank D. Vorselen, M. Villarreal, and J. Friedman for insightful discussions and help collecting preliminary data. E. Yurtsev, A. Conwill, and members of the Gore laboratory provided helpful comments on the manuscript. This work was supported by an NIH New Innovator Award (NIH DP2).

1. Korolev KS, Xavier JB, Gore J (2014) Turning ecology and evolution against cancer. *Nat Rev Cancer* 14(5):371–380.
2. Bryden J, Gill RJ, Mitton RAA, Raine NE, Jansen VAA (2013) Chronic sublethal stress causes bee colony failure. *Ecol Lett* 16(12):1463–1469.
3. Hirota M, Holmgren M, Van Nes EH, Scheffer M (2011) Global resilience of tropical forest and savanna to critical transitions. *Science* 334(6053):232–235.
4. Staver AC, Archibald S, Levin SA (2011) The global extent and determinants of savanna and forest as alternative biome states. *Science* 334(6053):230–232.
5. May RM (1977) Thresholds and breakpoints in ecosystems with a multiplicity of stable states. *Nature* 269(5628):471–477.
6. Lenton TM (2013) Environmental tipping points. *Annu Rev Environ Resour* 38(1):1–29.
7. Lever JJ, van Nes EH, Scheffer M, Bascompte J (2014) The sudden collapse of pollinator communities. *Ecol Lett* 17(3):350–359.
8. Scheffer M (2009) *Critical Transitions in Nature and Society* (Princeton Univ Press, Princeton).
9. Hughes TP, Carpenter S, Rockström J, Scheffer M, Walker B (2013) Multiscale regime shifts and planetary boundaries. *Trends Ecol Evol* 28(7):389–395.
10. Scheffer M, et al. (2009) Early-warning signals for critical transitions. *Nature* 461(7260):53–59.
11. Scheffer M, et al. (2012) Anticipating critical transitions. *Science* 338(6105):344–348.
12. Dakos V, et al. (2012) Methods for detecting early warnings of critical transitions in time series illustrated using simulated ecological data. *PLoS One* 7(7):e41010.
13. Kéfi S, et al. (2014) Early warning signals of ecological transitions: Methods for spatial patterns. *PLoS One* 9(3):e92097.
14. Kuehn C (2011) A mathematical framework for critical transitions: Bifurcations, fast–slow systems and stochastic dynamics. *Physica D* 240(12):1020–1035.
15. Lenton TM (2011) Early warning of climate tipping points. *Nat Clim Chang* 1(4):201–209.
16. Seekell DA, Carpenter SR, Cline TJ, Pace ML (2012) Conditional heteroskedasticity forecasts regime shift in a whole-ecosystem experiment. *Theor Ecol* 6(5):385–394.
17. Wang R, et al. (2012) Flickering gives early warning signals of a critical transition to a eutrophic lake state. *Nature* 492(7429):419–422.
18. Pal M, Pal AK, Ghosh S, Bose I (2013) Early signatures of regime shifts in gene expression dynamics. *Phys Biol* 10(3):036010.
19. van Nes EH, Scheffer M (2007) Slow recovery from perturbations as a generic indicator of a nearby catastrophic shift. *Am Nat* 169(6):738–747.
20. Carpenter SR, Brock WA (2006) Rising variance: A leading indicator of ecological transition. *Ecol Lett* 9(3):311–318.
21. Drake JM, Griffen BD (2010) Early warning signals of extinction in deteriorating environments. *Nature* 467(7314):456–459.
22. Dai L, Vorselen D, Korolev KS, Gore J (2012) Generic indicators for loss of resilience before a tipping point leading to population collapse. *Science* 336(6085):1175–1177.
23. Dai L, Korolev KS, Gore J (2013) Slower recovery in space before collapse of connected populations. *Nature* 496(7445):355–358.
24. Veraart AJ, et al. (2012) Recovery rates reflect distance to a tipping point in a living system. *Nature* 481(7381):357–359.
25. Carpenter SR, et al. (2011) Early warnings of regime shifts: A whole-ecosystem experiment. *Science* 332(6033):1079–1082.
26. Chen A, Sanchez A, Dai L, Gore J (2014) Dynamics of a producer-freeloader ecosystem on the brink of collapse. *Nat Commun* 5:3713.
27. Batt RD, Carpenter SR, Cole JJ, Pace ML, Johnson RA (2013) Changes in ecosystem resilience detected in automated measures of ecosystem metabolism during a whole-lake manipulation. *Proc Natl Acad Sci USA* 110(43):17398–17403.
28. Sornette D (2006) *Critical Phenomena in Natural Sciences: Chaos, Fractals, Self-organization and Disorder: Concepts and Tools (Springer Series in Synergetics)* (Springer, Berlin), 2nd Ed.
29. Guttal V, Jayaprakash C (2008) Spatial variance and spatial skewness: Leading indicators of regime shifts in spatial ecological systems. *Theor Ecol* 2(1):3–12.
30. Hohenberg P, Halperin B (1977) Theory of dynamic critical phenomena. *Rev Mod Phys* 49(3):435–479.
31. Wissel C (1984) A universal law of the characteristic return time near thresholds. *Oecologia* 65(1):101–107.
32. Dakos V, et al. (2008) Slowing down as an early warning signal for abrupt climate change. *Proc Natl Acad Sci USA* 105(38):14308–14312.
33. Hastings A, Wysham DB (2010) Regime shifts in ecological systems can occur with no warning. *Ecol Lett* 13(4):464–472.
34. Menck PJ, Heitzig J, Marwan N, Kurths J (2013) How basin stability complements the linear-stability paradigm. *Nat Phys* 9(2):89–92.
35. Boettiger C, Ross N, Hastings A (2013) Early warning signals: The charted and uncharted territories. *Theor Ecol* 6(3):255–264.
36. Dakos V, Carpenter SR, van Nes EH, Scheffer M (2014) Resilience indicators: Prospects and limitations for early warnings of regime shifts. *Philos Trans R Soc B Biol Sci* 370(1659):20130263.
37. Gore J, Youk H, van Oudenaarden A (2009) Snowdrift game dynamics and facultative cheating in yeast. *Nature* 459(7244):253–256.
38. Holling CS (1973) Resilience and stability of ecological systems. *Annu Rev Ecol Syst* 4(1):1–23.
39. Neubauer P, Jensen OP, Hutchings JA, Baum JK (2013) Resilience and recovery of overexploited marine populations. *Science* 340(6130):347–349.
40. Cole LES, Bhagwat SA, Willis KJ (2014) Recovery and resilience of tropical forests after disturbance. *Nat Commun* 5:3906.
41. Folke C, et al. (2004) Regime shifts, resilience, and biodiversity in ecosystem management. *Annu Rev Ecol Evol Syst* 35(1):557–581.
42. Gunderson LH (2000) Ecological resilience-in theory and application. *Annu Rev Ecol Syst* 31:425–439.
43. Standish RJ, et al. (2014) Resilience in ecology: Abstraction, distraction, or where the action is? *Biol Conserv* 177:43–51.
44. Dakos V, Nes EH, Scheffer M (2013) Flickering as an early warning signal. *Theor Ecol* 6(3): 309–317.
45. Boettiger C, Hastings A (2013) No early warning signals for stochastic transitions: Insights from large deviation theory. *Proc Biol Sci* 280(1766):20131372.
46. Boettiger C, Hastings A (2012) Quantifying limits to detection of early warning for critical transitions. *J R Soc Interface* 9(75):2527–2539.
47. Lade SJ, Gross T (2012) Early warning signals for critical transitions: A generalized modeling approach. *PLOS Comput Biol* 8(2):e1002360.
48. Courchamp F, Clutton-Brock T, Grenfell B (1999) Inverse density dependence and the Allee effect. *Trends Ecol Evol* 14(10):405–410.
49. Downing AS, van Nes EH, Mooij WM, Scheffer M (2012) The resilience and resistance of an ecosystem to a collapse of diversity. *PLoS One* 7(9):e46135.
50. Tang S, Allesina S (2014) Reactivity and stability of large ecosystems. *Front Ecol Evol* 2:21.
51. Neubert MG, Caswell H (1997) Alternatives to resilience for measuring the responses of ecological systems to perturbations. *Ecology* 78(3):653–665.
52. Ives AR, Carpenter SR (2007) Stability and diversity of ecosystems. *Science* 317(5834):58–62.
53. Grimm V, Wissel C (1997) Babel, or the ecological stability discussions: An inventory and analysis of terminology and a guide for avoiding confusion. *Oecologia* 109(3):323–334.
54. Haldane AG, May RM (2011) Systemic risk in banking ecosystems. *Nature* 469(7330): 351–355.
55. Costello EK, Stagaman K, Dethlefsen L, Bohannan BJM, Relman DA (2012) The application of ecological theory toward an understanding of the human microbiome. *Science* 336(6086):1255–1262.

Supporting Information

Relation between stability and resilience determines the performance of early warning signals under different environmental drivers

Lei Dai, Kirill S. Korolev, Jeff Gore

SI Appendix:

Supplementary Methods

Table S1 to S3

Text S1 to S3

Figure S1 to S10

Supplementary References

Supplementary Methods

Experimental protocols

We used a yeast strain derived from haploid cells BY4741 (mating type **a**, EUROSCARF). All experiments were performed in 200 μl batch culture on BD Falcon 96-well Microtest plates at 30°C using synthetic media supplemented with sucrose. Cultures were maintained in a well-mixed condition by growing in a shaker at 825 r.p.m. To avoid evaporation and contamination across wells, the plates were covered with Parafilm Laboratory Film. The 20% sucrose stock solution was filter-sterilized and stored with 1mM Tris buffer, pH 8.0, to prevent acid-catalyzed autohydrolysis. In all experiments we manually added a trace amount of glucose 0.001%, so that the monosaccharide concentration in sucrose stock (<0.0001%) can be ignored. Serial dilutions were performed daily (23 hours of growth) with variable dilution factors. Population densities were recorded each day before the serial dilution by measuring optical density at 620nm using a Thermo Scientific Multiskan FC microplate photometer and confirmed by plating (1).

For the two slowly deteriorating environments (Fig. 1), one driver was tuned for each experiment (Table S1): 1) Dilution factor was increased by 10% per day from 500 to over 2500 with [Sucrose] fixed at 2%; 2) [Sucrose] was decreased by 20% per day from 5% to 0.05% with Dilution factor fixed at 500. In the experiment with fixed environmental conditions (Fig. 2), concentrations of sucrose include 2.0, 1.0, 0.8, 0.6, 0.5, 0.4, 0.3, 0.2, and 0.16%, with Dilution factor fixed at 500; dilution factors include 500, 750, 1000, 1133, 1266, 1400, and 1600, with [Sucrose] fixed at 2%. 1% w/v sucrose is equal to 10g/L.

In the experiment to characterize the population dynamics under a third driver [NaCl], the concentrations of salt include 0, 100, 150, 200, 250, and 300mM. 1M [NaCl] is equal to 58.5g/L. The conditions were fixed and subject to Dilution factor at 500 and [Sucrose] at 2%. For this experiment, the optical density was measured at 600nm using a Thermo Scientific Varioskan Flash Multimode Reader.

Data analysis

Statistical indicators

Statistical indicators were calculated at each observation time over an ensemble of replicate populations. For the experiments with fixed environmental conditions, statistical indicators were calculated after the populations stabilized. The coefficient of variation was calculated as the sample standard deviation divided by the sample mean. The autocorrelation time τ was calculated as $\rho = e^{-1/\tau}$, where the lag-1 autocorrelation ρ was estimated by the Pearson's correlation coefficient between the population densities at subsequent days (1). The standard errors and confidence intervals of the indicators were given by bootstrap.

For the experiments with slowly deteriorating environments, because our sampling frequency was low relative to the rate of environmental changes, we did not detrend individual time series with insufficient time points. Instead, the statistics (CV, autocorrelation) were computed between replicate populations after subtracting the mean of replicates on each day. As the environment slowly deteriorated on each day, the yeast population relaxed to a new equilibrium, which should be close to the equilibrium of the environmental condition on the previous day (until the tipping point was crossed). The distribution among replicates and the resulting statistics (Fig. 1) could be complicated by the fact that all the populations were approaching the new equilibrium from above. However, our results at fixed environmental conditions do not have these complicated issues.

In all the analysis we ensured environmental homogeneity by excluding populations with systematic differences in density, which are presumably caused by errors in daily dilution. For the slowly deteriorating environments (Fig. 1), a subset of 20 replicate populations was used to calculate the indicators after excluding the populations on the edges of 96-well plates. Indicators calculated over the entire ensemble without imposing any selection display similar trends with larger increases (Fig. S6). Details on the analysis of populations under fixed dilution factors are described in supplementary reference (1). For the experiment with fixed sucrose concentrations (from 2.0% to 0.16%), the total number of replicate populations used for calculating indicators shown in Fig. 2 is 53, 47, 44, 32, 41, 30, 32, 27, 21, respectively. Indicators calculated over the entire ensemble without imposing any selection display similar trends with larger increases (Fig. S7).

We used bootstrap to estimate:

1) Confidence interval of indicators for populations in a slowly deteriorating environment (Fig. 1). Indicators were calculated based on 20 replicate populations. We resampled the 20 replicates 1000 times to obtain the 25-75% confidence interval of the indicators.

2) Standard errors of indicators for populations at fixed environmental conditions (Fig. 2, Fig. S2, Fig. S3). Indicators were calculated based on an ensemble of replicate populations over a span of 5 days. For each resampled distribution, there are two alternative methods: A) calculate the indicators for each day, and then average over 5 days; B) combine the data over 5 days into a single distribution, and then calculate the indicators. Both methods yielded similar results. The error bars shown were standard errors of indicators with resampling 1000 times using method A.

Fixed points and resilience

The stable and unstable fixed points can be identified as points at which the ratio of population densities between subsequent days equals one $n_{t+1}/n_t = 1$, n_t: population density at day. The cooperative growth of yeast in sucrose leads to two stable fixed points (i.e. bistability), with one non-zero stable fixed point for population survival n_{sfp} and the other one for population extinction. There is an unstable fixed point in between.

The unstable fixed points n_{ufp} were estimated by fitting the data points in the region where: 1) population density is lower than the value that gives the maximum growth, and higher than the detection limit (population density~5×10^2 cells/μl, below which the measurement becomes inaccurate); and 2) n_{t+1}/n_t (t=1 to 6) is in the range of [0.3 3] for data with fixed sucrose concentrations, or [0.5 2] for data with fixed dilution factors. The error bars shown in bifurcation diagrams correspond to 68% confidence interval given by bootstrap.

The (survival) stable fixed points n_{sfp} can be estimated by two alternative methods: A) the mean of replicate populations at equilibrium; B) locating the intersection of $n_{t+1} = n_t$ and data points near equilibrium on a n_{t+1} vs n_t plot. Both methods yielded similar results. Stable fixed points shown (Fig. 2) were estimated by the mean of replicate populations at equilibrium over five days (method A); the error bars correspond to standard errors of day-to-day variations.

Resilience r was calculated as the difference between the estimated stable (survival) and unstable fixed points, $r = n_{sfp} - n_{ufp}$. Given that the estimation of two fixed points were independent, standard errors of resilience were calculated by propagation of errors, $\Delta r = \sqrt{(\Delta n_{sfp})^2 + (\Delta n_{ufp})^2}$. Standard errors of unstable fixed points Δn_{ufp} were determined by bootstrap. Standard errors of stable fixed points Δn_{sfp} were computed from day-to-day variations.

Stability

In our study, we define stability λ as the recovery rate after a small perturbation near the stable fixed point, i.e. $x_{t+1} = e^{-\lambda} x_t$. $x_t \equiv n_t - n_{sfp}$ is the deviation from the stable fixed point on day *t*. Given the experimentally measured growth profile of yeast populations $n_{t+1} = f(\mathrm{n}_t)$, we can estimate stability by $\lambda = -\ln(f'(n_{sfp}))$, where $f'(n_{sfp}) = \left.\frac{df(n)}{dn}\right|_{\mathrm{n}_{sfp}}$ is the slope at the stable fixed point. This follows from Taylor expansion of the growth function

$$n_{t+1} \simeq f(n_{sfp}) + f'(n_{sfp})(n - n_{sfp})$$

Note that $f(n_{sfp}) = n_{sfp}$, it can be written as

$$x_{t+1} \simeq f'(n_{sfp}) x_t = e^{-\lambda} x_t$$

We estimated the slope at the stable fixed point $f'(n_{sfp})$ by fitting the data points with population density around the stable fixed point. Data points n_t (*t*=1 to 6) in the range of [$n_{sfp} \times 0.5$ $n_{sfp} \times 1.5$] and $n_{t+1} - n_t \geq -3.3 \times 10^4$ cells/μl were included in the fitting. The first condition was used to select data around the stable fixed point; the second condition was used to exclude some outliers. Error bars of stability correspond to standard errors given by bootstrap.

Simulations

We used a simple phenomenological model (1) to simulate the cooperative growth of yeast over

one day $n_{t+1} = f(n_t, \text{DilutionFactor}, \text{parameters})$. This model is based on two phases of daily growth: a slow exponential growth phase at low cell densities, followed by a logistic growth phase with a higher per capita growth rate at intermediate cell densities. This model has 5 parameters: T_{lag} is the lag time before yeast cells start to grow after being transferred into new media (the total time for daily growth is 23 hours). In the slow exponential phase, the population grows with a constant per capita growth rate γ_{low}. After the population reaches a threshold density N_c, the subsequent logistic growth is determined by γ_{high} ($\gamma_{high}>\gamma_{low}$) and the carrying capacity K.

$$\frac{1}{N}\frac{dN}{dt} = \begin{cases} \gamma_{low} & 0 < N < N_c \\ \gamma_{high}(1-\frac{N}{K}) & N_c \le N < K \end{cases}$$

Parameter values used for simulations in Fig. 5 are specified in Table S3.

Table S1. Experimental protocols of deteriorating environments.

Increase dilution factor by 10% per day		Reduce sucrose concentration by 20% per day	
Day	**Dilution Factor**	**Day**	**Sucrose (%)**
1-4	500	1-3	5.00
5	550.0	4	4.00
6	605.0	5	3.20
7	665.5	6	2.56
8	732.1	7	2.05
9	805.3	8	1.64
10	885.8	9	1.31
11	974.4	10	1.05
12	1071.8	11	0.84
13	1179.0	12	0.67
14	1296.9	13	0.54
15	1426.6	14	0.43
16	1569.2	15	0.34
17	1726.1	16	0.27
18	1898.7	17	0.22
19	2088.6	18	0.18
20	2297.5	19	0.14
21	2527.2	20	0.11
		21	0.09
		22	0.07
		23	0.06
		24	0.05

In each experiment we have a deteriorating-environment group and a constant-environment group. Starting on Day 5 (or Day 4), the daily dilution factor (or sucrose concentration) for populations in the deteriorating environment group was increased by 10% (or reduced by 20%) per day. The day underlined (Day 16 with an increasing dilution factor, or Day 20 with sucrose reduction) is the estimated day that the yeast populations crossed a tipping point (Fig. S1).

Table S2. Stability and resilience of dynamical systems.

	Stability	Resilience
Equivalent terms in literature	Recovery rate; Engineering resilience; Linear stability.	Ecological resilience; Basin stability.
Response to perturbations	Return rate to a stable fixed point after a small perturbation.	Tolerance of a large perturbation without shifting to an alternative stable state.
Mathematical definition	Dominant eigenvalue of Jacobian at the stable fixed point	Volume of basin of attraction
Potential/stability landscape	Curvature around the bottom (i.e. stable fixed point). It is a local property.	Difference in the state variable between the top (i.e. unstable fixed point) and the bottom (i.e. stable fixed point). It is a global property.
Metrics used in our study	$stability = -\ln(f'(n_{sfp}))$ $n_{t+1} = f(n_t)$ is the daily growth of yeast populations. $f'(n) \equiv \frac{df(n)}{dn}$	$resilience = n_{sfp} - n_{ufp}$ n_{sfp} : the stable fixed point (survival) n_{ufp} : the unstable fixed point

A one-dimensional dynamical system $\frac{dn}{dt} = g(n)$ can be represented by an effective potential $V(n)$, $g(n) = -\frac{dV(n)}{dn}$, where n is the state variable (i.e. population density). In our system, we define resilience as the maximal perturbation (i.e. number of individuals lost) a population can withstand without going extinct. Stability is defined as the return rate λ to the stable fixed point after small perturbations. $x_{t+1} = x_t e^{-\lambda}$, where $x_t \equiv n_t - n_{sfp}$ is deviation from the stable fixed point on day t.

Defining resilience for systems with higher dimensions is not always straightforward. Also, in systems where stochastic transitions between alternative stable states are common, an alternative metric for the health of an ecosystem is the expected lifetime of the state. In this situation the lifetime of the state could be used in place of the resilience as a way to compare the performance of early warning indicators under different environmental drivers.

Table S3. Parameter values used in simulations.

Parameter	Value
γ_{high}	0.4 hr^{-1}
γ_{low}	0.3 hr^{-1}
T_{lag}	2.97 hr
N_c	2.76×10^2 cells/μl
K	1.76×10^5 cells/μl
Dilution Factor (DF)	600

The above set of parameter values is the initial condition shown in Figure 5. Details of the model are specified in Supplementary Methods: Simulations.

For the anti-correlation path, the starting condition is (DF=1000, K=1.76×10^5 cells/μl), the ending condition is (DF=600, K=5.28×10^4 cells/μl). The decrease of DF and the decrease of K are both on a linear scale along this path; a total of 20 conditions are simulated.

Text S1. Scaling between stability and statistical indicators.

Statistical indicators such as CV and autocorrelation time characterize the size and timescale of fluctuations around a stable fixed point. Here we show that these indicators are reflections of changes in stability (i.e. recovery rate) in an AR(1) process (autoregressive model of order 1) (2).

Consider a stationary AR(1) process,

$$x_{t+1} = \rho x_t + \varepsilon_t$$

$x_t = n_t - n_{sfp}$ denotes the deviation from equilibrium population density on day t, $\varepsilon_t \sim N(0, \sigma^2)$ is Gaussian white noise. $\rho = e^{-\lambda}$ is determined by the recovery rate λ.

The variance of population density is

$$Var(x_t) = \frac{\sigma^2}{1-\rho^2} \overset{\lambda \to 0}{\simeq} \frac{\sigma^2}{2\lambda}$$

The autocorrelation of population density is

$$< x_t x_0 >= \rho^t = e^{-\lambda t} = e^{-t/T}$$

So the autocorrelation time T equals the recovery time,

$$T = \frac{1}{\lambda}$$

As populations approach a fold bifurcation, stability (the recovery rate) λ goes to zero, leading to an increase in statistical indicators. Given that standard deviation and autocorrelation time scale inversely with stability, their reciprocals (e.g. 1/CV) are sometimes used as alternative metrics of stability.

Text S2. Positive correlation between stability and resilience when close to a bifurcation.

Here we show that stability scales linearly with resilience near a fold bifurcation as a result of critical slowing down. Let's first look at the relation between resilience and the distance to the bifurcation. Given the quadratic shape of a fold bifurcation, when close to the bifurcation we have

$$|E-E_0| \sim r^2, \text{ or } r \sim |E-E_0|^{\frac{1}{2}}$$

E is the environmental driver (i.e. control parameter) with a fold bifurcation at E_0. $|E-E_0|$ is the distance to the bifurcation. Resilience r is the distance between the stable and unstable branches. Right at the fold bifurcation, resilience decreases to zero as the stable and unstable fixed points meet and "collide".

The scaling between stability and the distance to a bifurcation has been derived previously (3). For real eigenvalues (this is always the case for one-dimensional systems), it has been shown that the recovery time diverges with a critical exponent $\frac{1}{2}$

$$\frac{1}{\lambda} \sim |E-E_0|^{-\frac{1}{2}}, \text{ or } \lambda \sim |E-E_0|^{\frac{1}{2}}$$

Right at the fold bifurcation, stability λ decreases to zero (i.e. critical slowing down).

Combining the above results, we can see that close to a fold bifurcation stability scales linearly with resilience, $\lambda \sim r$.

The mathematical fact is that, stability and resilience are positively correlated only when the system is very close to the fold bifurcation. The real-world applications of critical slowing down as warning signals, however, assume that the relationship between stability and resilience is qualitatively preserved far from the bifurcation. To make such extrapolation requires validation from empirical observations in a variety of scenarios, including environmental deterioration caused by different drivers. In our experimental populations, we find a positive correlation between stability and relation over a wide range of conditions when a specific driver is tuned.

Text S3. A toy model with a cubic potential.

Here we aim to gain some intuition on the relation between stability and resilience from a toy model (Fig. S8A)

$$V(\mathrm{x}) = \alpha x^3 - \beta x^2$$

with $\alpha > 0, \beta \geq 0$. $V(\mathrm{x})$ is the effective potential of a one-dimensional dynamical system $\frac{dx}{dt} = g(\mathrm{x})$, where $\mathrm{g(x)} = -\frac{dV(\mathrm{x})}{dx}$ (4).

We can easily solve the fixed points of this model

$$g(\mathrm{x}) = x(2\beta - 3\alpha x) = 0$$

The unstable fixed point $x_{ufp} = 0$, the stable fixed point $x_{sfp} = \frac{2\beta}{3\alpha}$. This model has a transcritical bifurcation at $\beta_0 = 0$.

So we have resilience

$$r = x_{sfp} - x_{ufp} = \frac{2\beta}{3\alpha}$$

Stability is determined by

$$-\lambda = \left.\frac{dg(x)}{dx}\right|_{x_{sfp}} = -2\beta, \text{ or } \lambda = 2\beta$$

Now we plot contours of resilience and stability in the parameter space of (α, β) (Fig. S8B). As illustrated in Fig. 5 and Fig. S4C, this would help us identify scenarios in which the positive correlation between stability and resilience breaks down. For example, we can find two different scenarios of environmental deterioration before reaching the transcritical bifurcation: 1) a decrease in β with fixed α. This would lead to a decrease in both stability and resilience. 2) an increase in α followed by a decrease in β. In this case, when α is changed, resilience decreases while stability remains constant (i.e. zero correlation). As illustrated in Fig. 4, we can also visualize the

response of the system to different environmental changes as different paths on the stability-resilience diagram (Fig. S8C).

Additional notes:

1) The relation between stability and resilience presents a general framework to evaluate the performance of indicators based on critical slowing down and help us understand why they may fail. For example, in the toy model discussed in Menck *et al* (5), when approaching the bifurcation stability remains constant as resilience goes to zero. This scenario can be visualized as a horizontal line on the stability-resilience diagram (i.e. zero correlation).
2) Here we have not considered the mapping between model parameters and empirical environmental drivers. In principle, a single environmental driver may also lead to anti-correlation or zero correlation between stability and resilience.

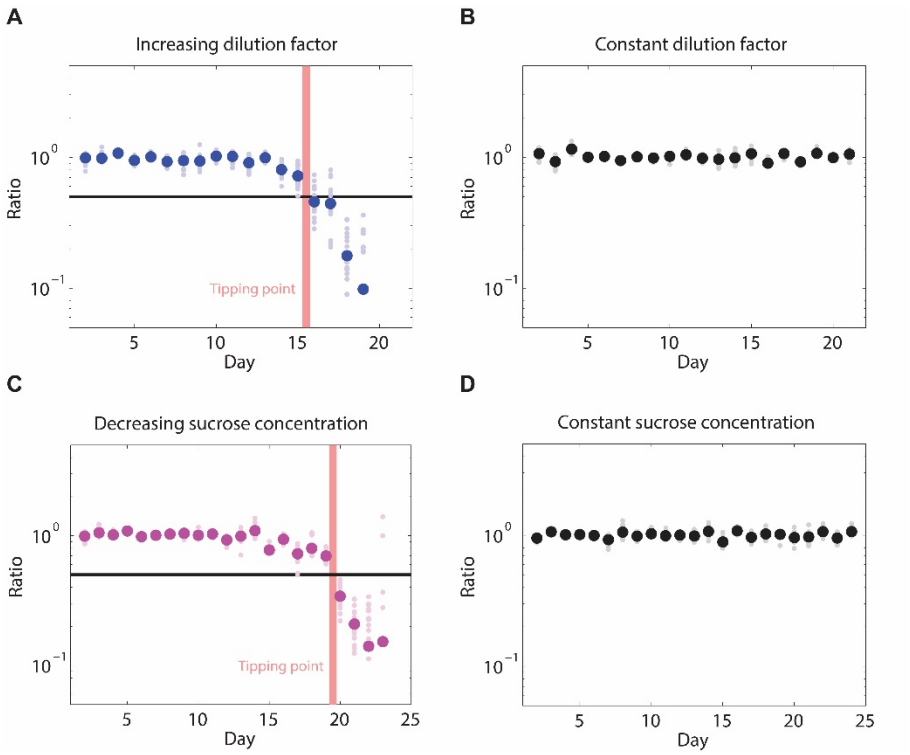

Figure S1. Estimation of the day when populations started to collapse in a deteriorating environment. (A) Deteriorating environment with increasing dilution factor over time; (B) Constant environment with dilution factor fixed at 500; (C) Deteriorating environment with a decreasing sucrose concentration over time; (D) Constant environment group with sucrose concentration fixed at 5%. Protocols of the deteriorating-environment experiments are specified in Table S1. Light dots: individual populations; dark dots: the mean ratio of 20 replicate populations; black line: threshold ratio at 0.5.

We estimated the day that the population crossed a tipping point by analyzing the ratio of population densities between subsequent days n_{t+1}/n_t . The control groups in constant environments maintained a ratio close to one. For the deteriorating-environment group, as the condition was deteriorated on a daily basis, the populations were constantly relaxing to a lower stable fixed point on each day, thus the ratio of population densities between subsequent days should be smaller than one. However, after crossing a tipping point (fold bifurcation), the stable fixed point would disappear and the population would enter a free fall to extinction with the ratio dropping significantly. We estimated the day that population collapse started as when the threshold ratio 0.5 was crossed. In the two different deteriorating environments, the estimates given by this

method (Table S1) matched well with the estimates given by the mapped bifurcation diagrams (Fig. 2): [Sucrose] ~ 0.12% and Dilution Factor ~ 1600. The estimated day when populations started to collapse after crossing the tipping point is marked in (A) and (C) (the same as in Fig. 1).

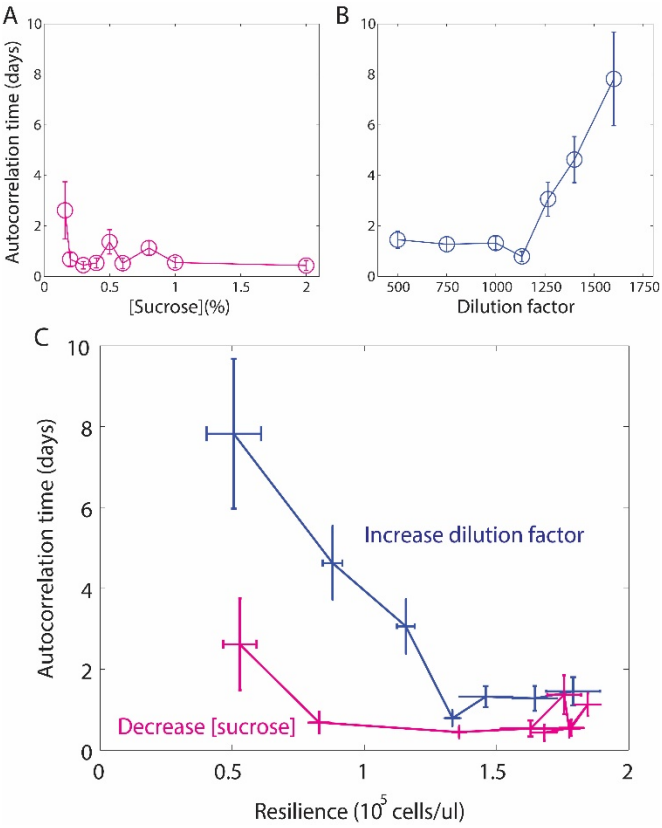

Figure S2. Performance of autocorrelation time under two different environmental drivers. (A, B) Autocorrelation time increased as environment deteriorated with decreasing sucrose concentration (A) or increasing dilution factor (B) (adapted from supplementary reference (1)). (C) To compare the performance of warning signals under different environmental drivers, we evaluated autocorrelation time as a function of resilience. Given that the same amount of resilience is lost, the increase in autocorrelation time was indeed more substantial with increasing dilution factor than with decreasing sucrose concentration. Error bars are standard errors given by bootstrap (Supplementary Methods).

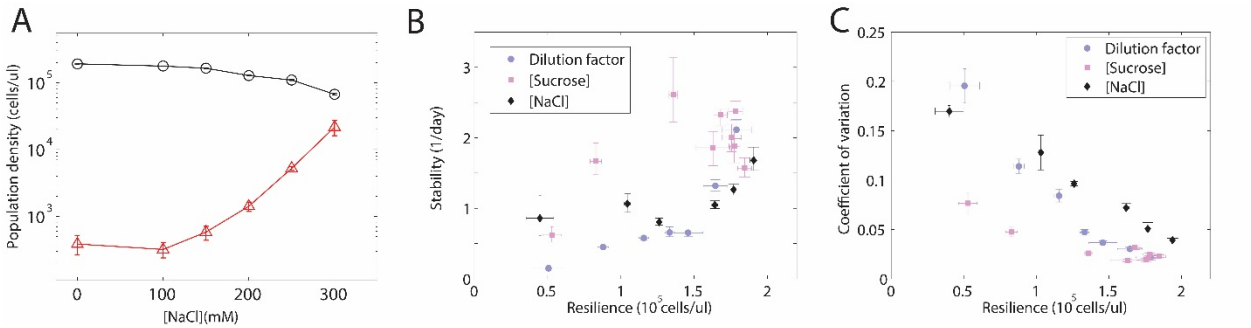

Figure S3. Stability-resilience relation and performance of warning indicators under a third environmental driver: osmotic stress caused by [NaCl]. (A) Bifurcation diagram for [NaCl] as an environmental driver. (B) Stability-resilience diagram. Our yeast populations lost both stability and resilience at higher concentration of salt, before eventually reaching a fold bifurcation. The exact path under this driver on the stability-resilience diagram was observed to be between the two paths of dilution factor and sucrose. The estimation of resilience and stability was performed in a similar fashion as for the other two drivers. Data points with n_{t+1}/n_t (t=1 to 3) in the range of [0.1 10] are used to fit unstable fixed points. The stable fixed points are estimated by method B and error bars correspond to standard errors given by bootstrap (Supplementary Methods). (C) CV of yeast populations under osmotic stress are compared to the other two drivers as "indicators of resilience". As the environment deteriorates with an increasing concentration of salt, we found that changes in CV as a function of resilience were intermediate among the three drivers. CV was calculated among replicate populations over a span of 3 days after population density reached equilibrium; error bars correspond to standard errors of day-to-day variations. A filtering procedure to ensure environmental homogeneity was performed in a similar fashion as under the other drivers (Supplementary Methods).

We note that the highest [NaCl] used in our experiment (~0.3M or 20g/L) is well below the lethal concentration (6). Adaptation of yeast under these salt concentrations at the timescale of our experiment (less than a week) is expected to be minimal (7, 8), so any heterogeneity introduced by adaptation should be insignificant in comparison to the true variation among the replicate populations.

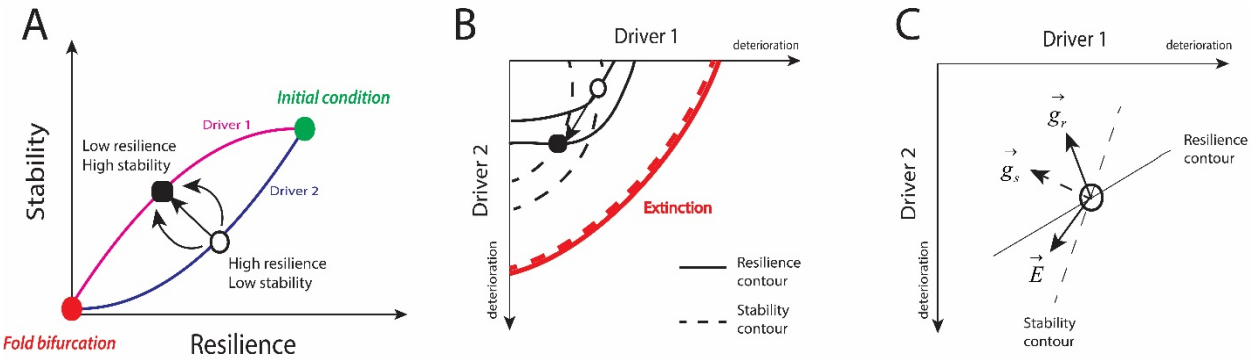

Figure S4. Changes in stability and resilience can be anti-correlated when multiple environmental drivers are involved. (A) Stability-resilience diagram. Given that different drivers lead to different paths on the stability-resilience diagram, we can readily find conditions with a trade-off between stability and resilience. For example, one condition (open black dot) has high resilience and low stability, while the other (filled black dot) has low resilience and high stability. (B) An anti-correlation path can be visualized in the parameter space of two drivers. The contours end at the fold bifurcation as both stability and resilience are reduced to zero (they cannot be negative). Close to the fold bifurcation, stability scales linearly with resilience (Text S2) so their contours tend to parallel (red lines). Farther away from the bifurcation, however, contours of stability and resilience can intersect and the positive correlation between the two properties may break down. (C) An intersection of resilience contour and stability contour. $\vec{g}_r$ and $\vec{g}_s$ denote the gradient of resilience and stability, respectively. $\vec{E}$ represents an environmental change involving two drivers. When $\vec{g}_r \cdot \vec{E} < 0$ and $\vec{g}_s \cdot \vec{E} > 0$, a decrease in resilience will be accompanied by an increase in stability.

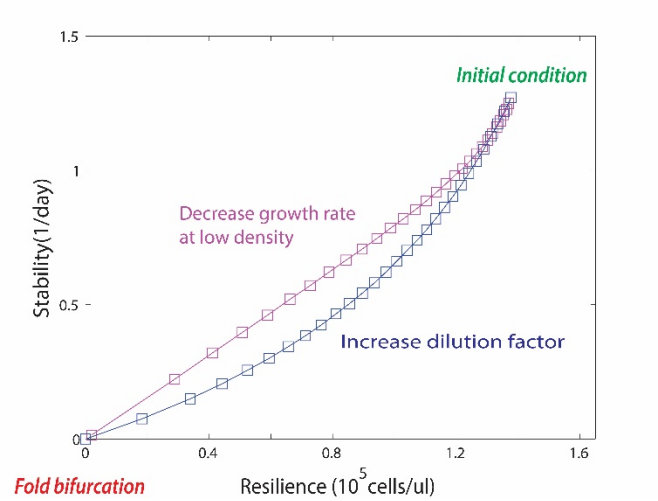

Figure S5. Simulated stability-resilience relation by tuning the growth rate at low cell density in a phenomenological model of yeast growth. In addition to the simulations corresponding to varying dilution factor and carrying capacity (Fig. 5A), we explored another scenario in which the growth rate during slow growth phase γ_{low} (Supplementary Methods) was decreased, which also led to a different path on stability-resilience diagram. In our experiment, lowering the sucrose concentration would limit the carrying capacity as well as how fast yeast cells grow at low cell densities. Thus, the outputs of our model were consistent with the experimental observation that tuning sucrose concentration led to a less convex path than tuning dilution factor.

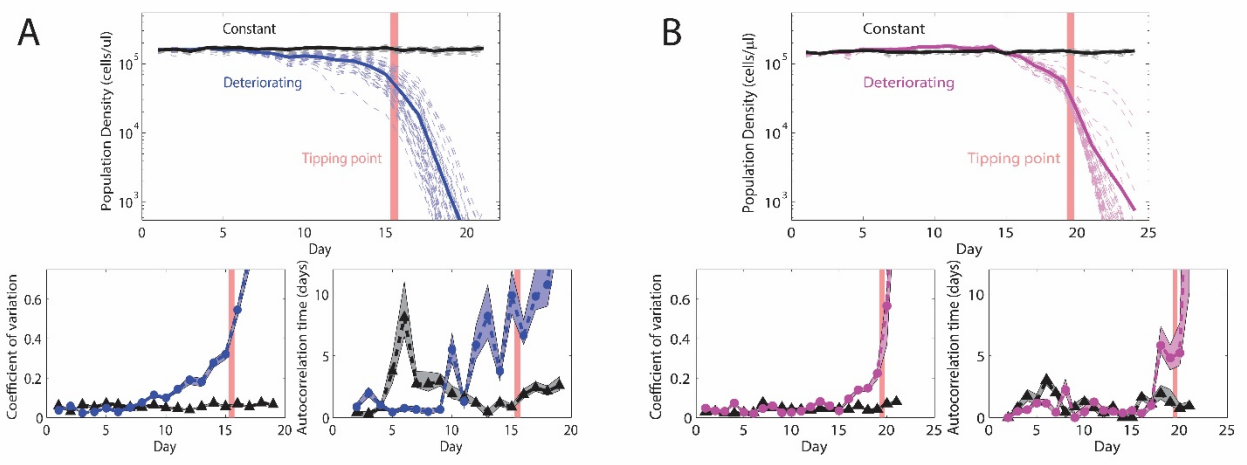

Figure S6. With an increasing dilution factor, statistical indicators calculated over either the entire ensemble or a subset of populations showed similar trends. Population density and statistical indicators based on the entire ensemble of 36 replicate populations in a deteriorating environment with (A) an increasing dilution factor or (B) decreasing sucrose concentration. In Fig. 1, a subset of 20 replicate populations was used to calculate the indicators after excluding the populations on the edges of 96-well plates. Conventions for symbols and confidence intervals are the same as defined in Fig. 1.

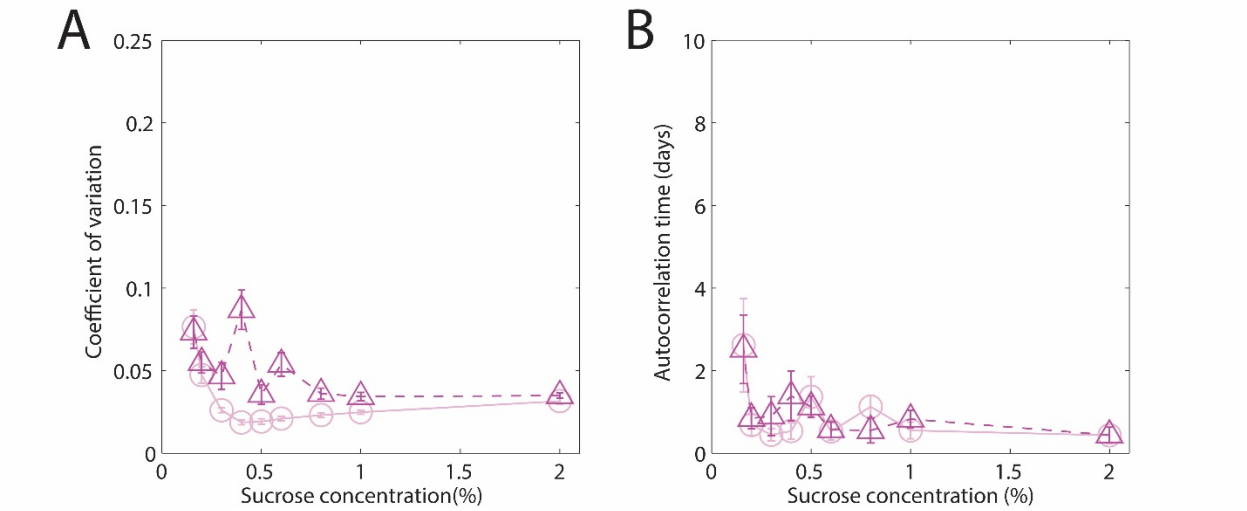

Figure S7. With decreasing sucrose concentrations, statistical indicators calculated over either the entire ensemble or a subset of populations showed similar trends. Comparison between statistical indicators calculated using all the replicate populations (triangles) and using a subset of populations (circles, data shown in Fig. 2 and S2) under a range of fixed sucrose concentrations. In the subset of populations, wells on the edges of 96-well plates or displaying large jumps of population density (>2×10^4 cells/μl) between subsequent days, presumably caused by pipetting errors, were excluded.

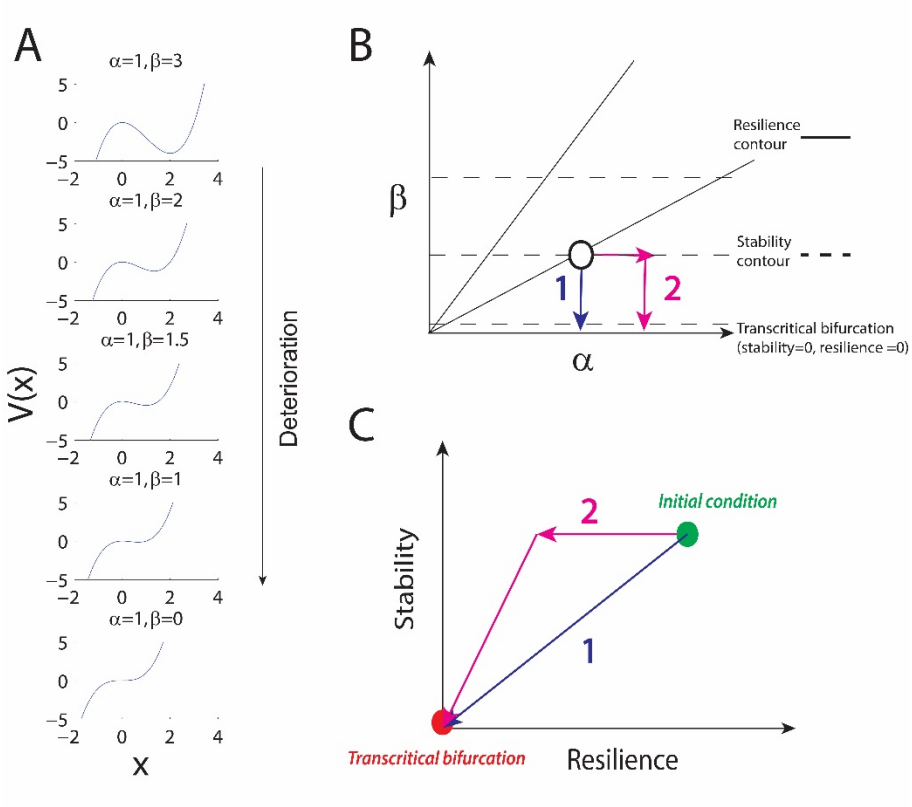

Figure S8. Relation between stability and resilience in a toy model with a cubic potential. (A) $V(\mathrm{x}) = \alpha x^3 - \beta x^2$ is the effective potential. This model has a transcritical bifurcation at $\beta_0 = 0$. (B) Contours of resilience and stability in the parameter space of (α, β). We illustrate wo scenarios of environmental deterioration before reaching the transcritical bifurcation: 1) a decrease in β with fixed α. This would lead to a decrease in both stability and resilience. 2) an increase in α followed by a decrease in β. In this case, when α is changed, resilience decreases while stability remains constant (i.e. zero correlation). (C) The response of the system to different environmental changes can be visualized as different paths on the stability-resilience diagram. In the second scenario, as the environment deteriorates the positive correlation between stability and resilience does not always hold.

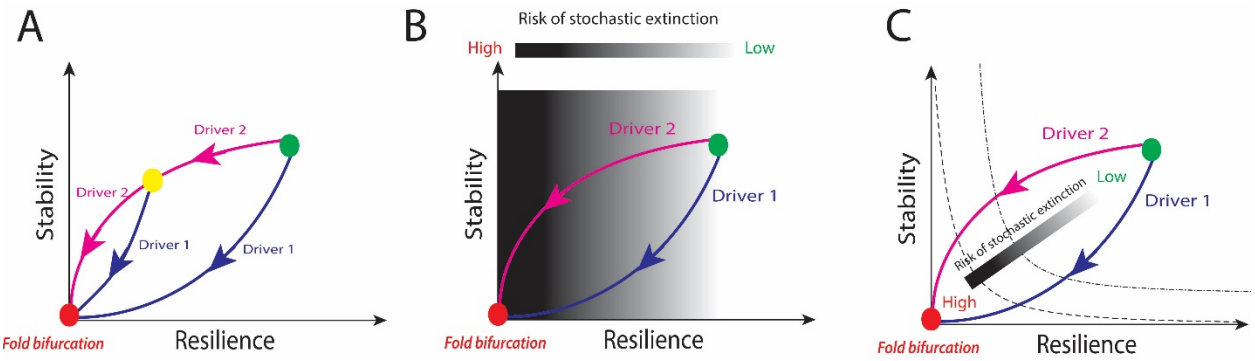

Figure S9. The stability-resilience relation reflects intrinsic difference between environmental drivers and determines the utility of critical slowing down as resilience indicators. (A) We expect more loss of stability and thus a larger increase in statistical indicators along a more convex path on the stability-resilience diagram (Driver 1) than a concave path (Drive 2). This observation does not depend on the location of the starting condition (green dot or yellow dot). In the context of our system, this means that if at any time the cause of the environmental deterioration shifts from nutrient limitation to a rising death rate we will observe a comparatively more rapid loss of stability than loss of resilience. (B) Warning indicators need to be observed before resilience becomes too small, as large environmental perturbations (i.e. external forcing) will occasionally push systems to transition towards collapse before the deterministic bifurcation. Given this need to maintain a minimal resilience, the early warning indicators based on loss of stability will be more effective for Driver 1 as compared to Driver 2 as a result of their different paths on the stability-resilience diagram. In this scenario, a large environmental perturbation happens once in a while and could push the population below the extinction threshold (i.e. the unstable fixed point) if resilience is low. (C) If extinctions are driven by stochastic fluctuations in population size (the source of stochasticity could be demographic or environmental noise), then in the limit of small noise the risk of extinction depends on the height of potential well (9), which scales as ~(stability)×(resilience)^2. In this case, changes in Driver 1 would also lead to more loss of stability (i.e. strong warning signals) given the same increase in the risk of extinction. Thus, our finding on stability-resilience relation holds true for both scenarios of extinction before the deterministic bifurcation (either due to large but rare perturbations like external forcing events, or small but frequent perturbations like demographic and/or environmental noise), despite the fact that the risk of extinction would scale differently with resilience and stability.

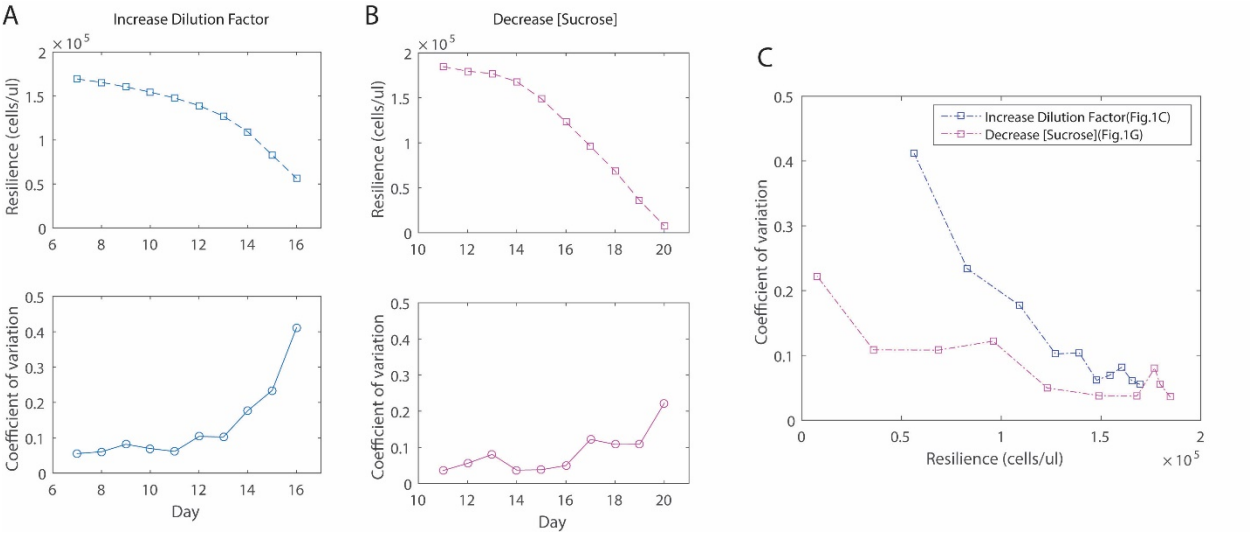

Figure S10. The varying performance of early warning indicators in two slowly deteriorating environments can be explained to some extent by the stability-resilience relation. Based on interpolation of the bifurcation diagrams (Figure 2), we plotted how resilience changed over time (ten days before crossing the estimated tipping point) in the slowly deteriorating environments (panel A: increasing Dilution Factor, Figure 1A-D; panel B: decreasing [Sucrose], Figure 1E-H). Comparing the time series of resilience and warning indicators (e.g. CV), we could see that given the loss of resilience the increase in CV is more dramatic under increasing dilution factor. The varying performance of CV (panel C) is consistent with our observation at constant environmental conditions (Figure 2). Although we cannot fully disentangle the possible influence by the rate of environmental deterioration, the stability-resilience relation can explain to some extent the different performance of warning indicators observed in two slowly deteriorating environments (Figure 1).

Supplementary References

1. Dai L, Vorselen D, Korolev KS, Gore J (2012) Generic indicators for loss of resilience before a tipping point leading to population collapse. *Science* 336(6085):1175–7.

2. Scheffer M, et al. (2009) Early-warning signals for critical transitions. *Nature* 461(7260):53–9.

3. Wissel C (1984) A universal law of the characteristic return time near thresholds. *Oecologia* 65(1):101–107.

4. Strogatz SH (1994) *Nonlinear dynamics and chaos: with applications to physics, biology, chemistry, and engineering* (Westview Press).

5. Menck PJ, Heitzig J, Marwan N, Kurths J (2013) How basin stability complements the linear-stability paradigm. *Nat Phys* 9(2):89–92.

6. Bell G, Gonzalez A (2009) Evolutionary rescue can prevent extinction following environmental change. *Ecol Lett* 12(9):942–8.

7. Samani P, Bell G (2010) Adaptation of experimental yeast populations to stressful conditions in relation to population size. *J Evol Biol* 23(4):791–6.

8. Bell G, Gonzalez A (2011) Adaptation and evolutionary rescue in metapopulations experiencing environmental deterioration. *Science* 332(6035):1327–30.

9. Gardiner C (2009) Stochastic Methods - A Handbook for the Natural and Social Sciences.